Check for updates

Original Research Article

Surface Defect Engineering on CeO_2 Nanoparticles Through Green Process Using *Vitex trifolia* Leaf Extract and Their Structural, Optical, and Biomedical Application

Pharmacognosy Magazine
22(3) 872–884, 2026
© The Author(s) 2025
Article reuse guidelines:
in.sagepub.com/journals-permissions-india
DOI: 10.1177/09731296251391939
journals.sagepub.com/home/phm

Abdullah A. Alarfaj[1], Abdurahman H. Hirad[1], Akon Higuchi[2,3], Murugan A. Munusamy[1] and Suresh Kumar Subbiah[4]

Abstract

Background: Nanotechnology based research offers a favorable method to address breast cancer and bacterial resistance, two serious global health challenges. Breast cancer is one of the most commonly diagnosed tumors global and is an important cause of death among women.

Objectives: This study presents the synthesis of cerium dioxide nanoparticles (CeO_2 NPs) using Vitex trifolia leaf extract in an eco-friendly approach. This process results in the CeO_2 NPs becoming biocompatible. This approach addresses environmental concerns by utilizing safe, non-toxic chemicals and reducing preparation costs, making the NPs suitable for healthcare applications.

Materials and Methods: Characterization techniques, including XRD, FTIR, DLS, UV-Vis, FESEM, EDAX, PL, and antimicrobial as well as anti-cancer analysis, were employed.

Results: XRD patterns revealed a cubic structure for the CeO_2 NPs, while morphological observations showed agglomerated uniform nano-belt-like structures with uniform grain boundaries. The agar well diffusion technique demonstrated the antimicrobial activities of CeO_2 NPs against human pathogens, suggesting their potential as nano-antibiotics. In vitro tests on MDA-MB-231 cells found that the synthesized CeO_2 NPs had minimal toxicity. However, they did show potential to be cytotoxic, resulting in increased lethality against the cancer cells. The AO/EtBr dual staining method was employed to assess cell viability, confirming that CeO_2 nanoparticles induced apoptotic cell death in MDA-MB-231 cells.

Conclusion: These findings proved that CeO_2 NPs inhibit cell growth and cause apoptosis in breast cancer cells and are employed as a tool for individualized therapy for targeting and eliminating breast cancer cells.

Keywords

Vitex trifolia, cerium dioxide, nanoparticles, anti-bacterial activity, apoptotic cell death

Received 29 April 2025; **revised** 06 September 2025; **accepted** 18 September 2025

Introduction

Recently, the biggest threat to global public health has been microbial resistance to the antibiotics that are currently in use (Majumder et al., 2020). Antibiotics are the human defense mechanism against infections; however, their effectiveness has been diminished due to overuse. The alarming rate of antibiotic resistance around the world has increased treatment costs and mortality rates, endangering human health (AlSheikh et al., 2020). Reports indicate that 10 million deaths per year will result from drug-resistant illnesses by 2025. Most gram-positive (G+) and gram-negative (G−) bacterial infections cause mortality and chronic infections. Antibiotic resistance has evolved, leading to a significant rise in the burden of disease (Wang et al., 2017). The World Health Organization (WHO) counsels about the seriousness of the

[1]Department of Botany and Microbiology, College of Science, King Saud University, Riyadh, Saudi Arabia
[2]School of Ophthalmology and Optometry, Eye Hospital, Wenzhou Medical University, Wenzhou, Zhejiang, China
[3]Department of Chemical and Materials Engineering, National Central University, Jhongli, Taoyuan, Taiwan
[4]Centre for Stem Cell-Mediated Advanced Research, Saveetha Dental College and Hospitals, Saveetha Institute of Medical and Technical Sciences, Saveetha University, Chennai, Tamil Nadu, India

Corresponding authors:
Murugan A. Munusamy, Department of Botany and Microbiology, College of Science, King Saud University, Riyadh 11451, Saudi Arabia.
E-mail: ammurugan11@gmail.com
Suresh Kumar Subbiah, Centre for Stem Cell-Mediated Advanced Research, Saveetha Dental College and Hospitals, Saveetha Institute of Medical and Technical Sciences, Saveetha University, Chennai, Tamil Nadu 600077, India.
E-mail: sureshkudsc@gmail.com

Creative Commons Non Commercial CC BY-NC: This article is distributed under the terms of the Creative Commons Attribution-NonCommercial 4.0 License (http://www.creativecommons.org/licenses/by-nc/4.0/) which permits non-Commercial use, reproduction and distribution of the work without further permission provided the original work is attributed as specified on the SAGE and Open Access pages (https://us.sagepub.com/en-us/nam/open-access-at-sage).

antibiotic resistance crisis (Ventola, 2015). Therefore, alternative treatments such as novel nanomedicines could help in the treatment of bacterial infection-related diseases.

Nanoparticles (NPs) have exhibited improved anti-bacterial properties; metal oxide NPs in particular are a promising solution for biomedical applications because of their adaptability to specific dimensions, high stability, ease of synthesis, and incorporation into hydrophobic and hydrophilic systems (Nikolova & Chavali, 2020). cerium dioxide NPs (CeO_2 NPs), with their mixed valence states, exhibit greater anti-bacterial activity than zinc oxide (ZnO) and titanium dioxide NPs (TiO_2 NPs) (Zhang et al., 2019). According to Ravishankar et al. (2015), the CeO_2 NPs have anti-bacterial activity against *Pseudomonas aeruginosa* and *Escherichia coli* (Lan et al., 2018). The size, shape, polar surface, surface area, and other characteristics of CeO_2 NPs typically influence their anti-bacterial activity. Furthermore, the electrostatic attraction of NPs and bacterial cells also contributes to their bactericidal activity. Such attraction suppresses bacterial growth, increases the level of reactive oxygen species (ROS), and consequently leads to cell death (Arumugam et al., 2015). In addition to CeO_2 NPs, hybrid chitosan-CeO_2 NPs demonstrate exceptional anti-bacterial characteristics by breaking cell membranes, resulting in cell death. However, this is only achievable at high concentrations of this hybrid nanoparticle (Senthilkumar et al., 2017).

In this study, *Vitex trifolia* leaf extract was used to synthesize CeO_2 NPs using a green method. *V. trifolia* (L.) is a shrub that grows throughout Asia and the Pacific, including French Polynesia, Australia, China, Indonesia, and the Philippines. The larvicidal activities of *V. trifolia* leaf extracts against the mosquito *Culex quinquefasciatus* have been demonstrated (Kannathasan et al., 2007). Furthermore, extracts of ethanol from the *V. trifolia* leaves had a moderate effect on both pathogenic bacteria (Hossain et al., 2001). Secondary metabolites of plants having functional groups, like phenols, flavonoids, and carbohydrates, may be able to stabilize metal ions for environmentally friendly NPs production (Yasir et al., 2017). CeO_2 NPs were synthesized through biochemical synthesis with natural compounds as reagents. The challenges of utilizing this metal oxide safely and effectively for biomedical applications are addressed, and biocompatible materials are produced (Charbgoo et al., 2017). Neogambogic acid combined with ceria NPs (NGA-CNPs) is utilized as an adjunct to radiotherapy, enhancing the effectiveness of breast cancer treatment (Chen et al., 2015).

When green-synthesized nanoceria with different surface charges is employed to treat cancer and normal cells, it exhibits variable surface charge-dependent localization of nanoceria in normal and tumor cells; such localization plays a crucial role in the toxicity of the NPs (Asati et al., 2010). In another research, it was observed that Fe-doped CNPs exhibited certain cytotoxic effects against MCF-7 cells (Rahdar et al., 2019). Previous research has reported that *V. trifolia* extracts have larvicidal, anti-inflammatory, anti-diabetic, anti-microbial, anti-asthmatic, antioxidant, anti-histaminic, hepatoprotective, and anti-cancer effects (Chan et al., 2018; Kamal et al., 2022). *V. trifolia* was found to produce a positive influence on human myeloid leukemia K562 cells by inducing apoptosis, as well as inhibiting the progression of the cell cycle at the G2/M phase in traditional Chinese medicine. Flavonoids are the constituents of the plant that induce apoptosis (Li et al., 2005). In the present work, the systematic characterization of X-ray diffraction (XRD), Fourier transform infrared spectroscopy (FT-IR), dynamic light scattering (DLS), ultraviolet–visible spectroscopy (UV–vis), field emission scanning electron microscopy (FESEM), energy dispersive X-ray analysis (EDAX), and photoluminescence spectroscopy (PL) of the as-produced CeO_2 NPs. Anti-bacterial assay results of CeO_2 nanobelts prepared via green methods presented an identical level of anti-bacterial activity to traditional antibiotics amoxicillin. This has implied that CeO_2 does significantly play a part in the fight against bacterial activities. In this study, the cytotoxic and antioxidant activity of CeO_2 NPs on MDA-MB-231 cells via eco-friendly methods has been evaluated.

Materials and Methods

Synthesis of V. trifolia Plant Extract

The extract was prepared from *V. trifolia* leaves, which were collected during the summer, cleaned, and deionized before being added to 10 g of fresh and cut leaves. The magnetic stirrer was then used to boil the extract for 20 min at 80°C. After filtering, the liquid phase was kept for later use in the preparation of NPs at 25°C.

Green Synthesis of CeO_2 NPs

This study included combining 100 mL of *V. trifolia* leaf extract with a 0.1 M cerium oxide hexahydrate solute, using magnetic agitation for 4 h, followed by cooling, centrifugation, dehydration at 120°C for 2 h, and galvanization at 800°C for 5 h. The green-synthesized CeO_2 NPs were then utilized for additional characterization, and a pictorial illustrating the formation of the green NPs can be found in Figure 1 (Chinnasamy et al., 2024; Fesenko et al., 2020).

Characterization Techniques

CeO_2 NPs were analyzed within the study using an XRD, showing diffraction peaks in the range of 20°–80°. The scanning electron microscope (Carl Zeiss Ultra 55 FESEM) was operated together with the energy-dispersive X-ray spectrometry (EDX) to study the NPs. The size of the particles was obtained using the Nano-Plus device, while a xenon lamp and a Perkin–Elmer spectrometer were used for the FT-IR study (Chinnasamy et al., 2024; Fesenko et al., 2020).

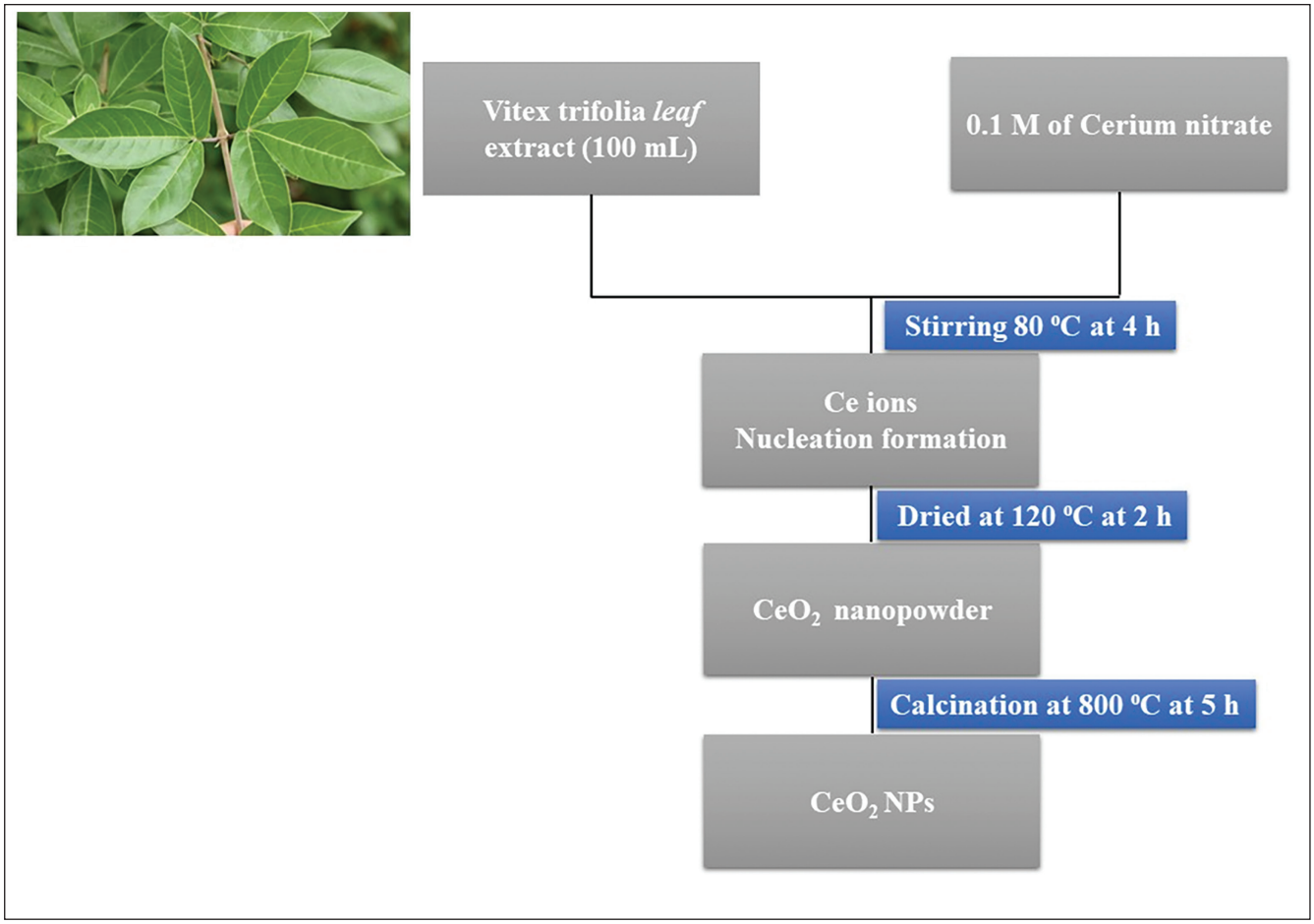


Figure 1. Flowchart for the Synthesis of Cerium Dioxide Nanoparticles (CeO_2 NPs) via a Green Process Using *Vitex trifolia* Leaf Extract as a Reducing and Capping Agent.

Antioxidant Activity

The 2,2-diphenyl-1-picrylhydrazyl (DPPH) radical scavenging properties of the CeO_2-NPs were assessed using a standard technique (Soren et al., 2015). In this procedure, a 10 mL solution of 0.2 mg/mL DPPH in ethanol was prepared in an amber-colored glass bottle. The CeO_2-NPs, produced in ethanol and well-distributed, were then added to achieve a final concentration of 4 mg/mL. The color change from dark violet to pale yellow caused by free DPPH radical scavenging was observed at 517 nm at various periods. The dose of CeO_2 NPs used in this study was determined based on preliminary dose–response assessments, supported by relevant literature and established toxicological guidelines, to ensure scientific rigor, reproducibility, and the reliability of the toxicity evaluation (Chinnasamy et al., 2024). The scavenging level of DPPH was also determined by diverse doses of CeO_2-NPs (3.13–200 mg/mL) for 1 h, and outcomes were revealed as a percentage of DPPH scavenged, which is calculated by the formula of % of DPPH radical scavenged = OD (Control) − OD Test/OD (Control) × 100 (Karthikeyan et al., 2022; Soren et al., 2015).

Anti-microbial Activity

The anti-microbial properties of the green-fabricated CeO_2 NPs were evaluated against *Staph aureus*, *Streptococcus pneumonia*, *Bacillus subtilis*, *Klebsiella pneumonia*, *P. aeruginosa*, *Vibrio cholerae*, as well as *Candida albicans*, utilizing the diffusion method. The wells were developed and then filled with varying concentrations of CeO_2 NPs along with a positive control that inhibits both bacteria and fungi (ampicillin for bacteria and fluconazole for fungi). The purpose of the study was to determine whether CeO_2 NPs could improve the anti-microbial qualities of different bacteria (Karthikeyan et al., 2022).

3-(4,5-Dimethylthiazol-2-yl)-2,5-Diphenyltetrazolium Bromide (MTT) Assay

An MTT assay was used to evaluate the cytotoxic profile of CeO_2 NPs. Different dosages of CeO_2 NPs were applied to MDA-MB-231 and MCF-10A cells. Following treatment, cells were mixed with MTT and cleaned with phosphate-buffered saline (PBS). After digesting formazan crystals with

dimethyl sulfoxide (DMSO), absorbance at 570 nm was found. The outcomes demonstrated the potential cytotoxicity of the NPs and were compared with the positive control doxorubicin (Sarathbabu et al., 2019).

Dual Staining

MDA-MB-231 cells were collected, then placed into six-well plates and covered with clear, sterile coverslips. After being treated for 24 h with 20 and 40 µg of CeO_2 NPs, the cells were kept at 37°C for 15 min with 1 µM of acridine orange (AO)/ethidium bromide (EtBr). Finally, the dyed MDA-MB-231 cells were examined under a fluorescence microscope to see how they responded to the AO/EtBr dye (Sarathbabu et al., 2019).

Estimation of ROS

For ROS analysis and quantification, MDA-MB-231 cells were exposed to 20 and 40 µg of CeO_2 NPs for a full day. Afterward, 10 µM dichloro-dihydro-fluorescein diacetate (DCFH-DA) was used to stain the MDA-MB-231 cells after they had been cleaned with PBS. Ultimately, utilizing a fluorescent microscope (Nikon Eclipse Ti microscope) with the appropriate excitation and emission wavelengths (485 nm/535 nm) (Munusamy et al., 2024).

Mitochondrial Membrane Potential (MMP) Analysis

The MDA-MB-231 cells were plated at a density of 2×10^5 cells/well in a 24-well plate, which then underwent experimental protocols. MMP, with Rh123 staining, was set up. MDA-MB-231 cells were incubated in the culture at 37°C for 30 min in the dark with 10 mM Rh 123. After three PBS rinses, the cells were visualized under a fluorescent microscope, Nikon Eclipse Ti microscope (Munusamy et al., 2024).

Statistical Analysis

All statistical analyses were performed using Statistical Package for the Social Sciences (SPSS) software version 12.0 (SPSS Inc., Chicago, IL, USA). Data were expressed as the mean ± standard deviation (SD). To assess the statistical significance among multiple groups, a one-way analysis of variance (ANOVA) was conducted. Following ANOVA, Tukey's honestly significant difference (HSD) *post hoc* test was applied to identify specific differences between the group means.

Results and Discussion

XRD Study

Using XRD at an angle of 2θ between 20° and 80°, the structural identification of green-synthesized CeO_2 NPs was determined (Figure 2a). The crystallinity of CeO_2 NPs was proven by a unique diffraction peak. In the fluorite structure of CeO_2, Ce^{4+} is surrounded by eight equivalent O^2 ions, forming the cube's corner, with each O_2 connected to four Ce^{4+} ions (Deshpande et al., 2005; Li et al., 2009). The peaks of CeO_2 NPs at (111), (200), (220), (311), (222), (400), (331), and (420) correlate to the following coordinate systems: 28.56°, 33.09°, 48.50°, 57.40°, 59.07°, 69.45°, 76.70°, and 79.09°.

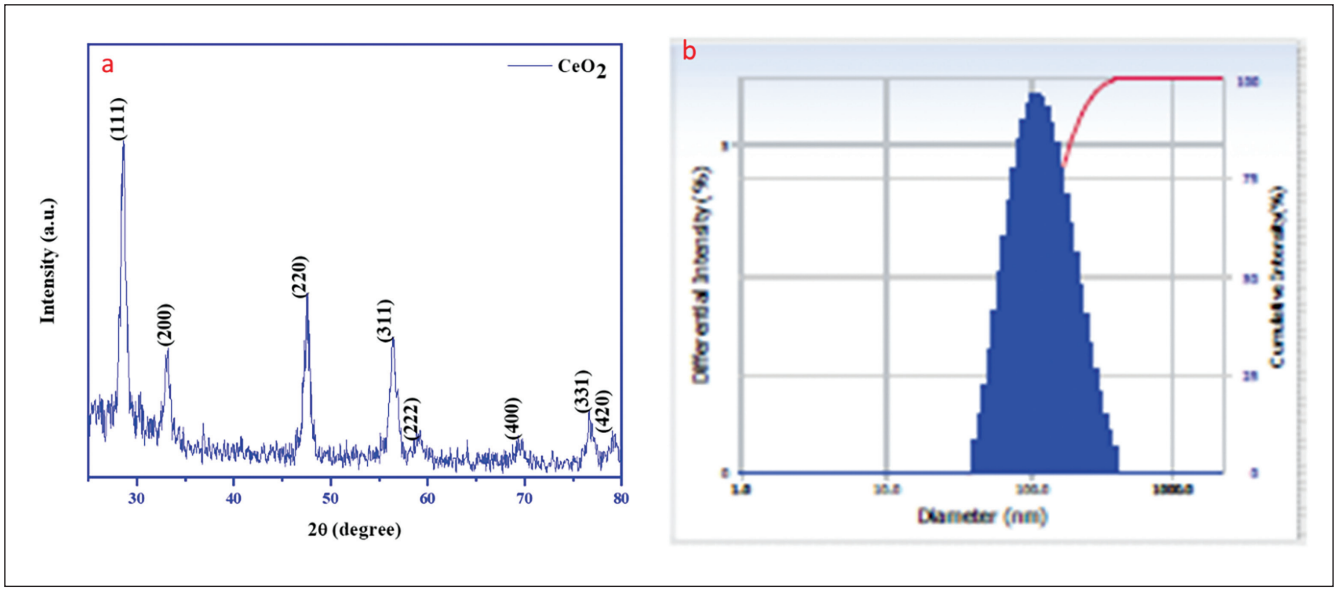


Figure 2. An X-ray Diffraction (XRD) Analysis (a) and Dynamic Light Scattering (DLS) Spectrum (b) of Cerium Dioxide Nanoparticles (CeO_2 NPs) are Shown. Three Replicates were Performed, and Representative Images are Shown.

The observed pattern is consistent with CeO_2 in its cubic fluorite form (JCPDS-340394). The cubic structure of CeO_2's "a" lattice constant was evaluated using

$$1/d^2 = (h^2 + k^2 + l^2)/a^2$$

The average crystalline size was determined using Debye Scherrer's relation $D = \frac{k\lambda}{\beta_{D\cos\theta}}$ (Karthikeyan et al., 2022), and the XRD planes show that CeO_2 NPs have a cubic shape with a lattice constant (a) value of 5.436 Å. where λ is the XRD wavelength (1.5406 nm), β is the FWHM in radians, θ is the Bragg's angle, and k is the shape factor of 0.96. For CeO_2 NPs, the typical crystallographic size is 34 nm.

DLS Analysis

The synthesized CeO_2 NPs size ranges were determined via DLS analysis (Ningaraju et al., 2019), with the outcomes displayed in Figure 2b. According to our findings, the produced CeO_2 NPs have an average size of 114 nm and range in size from 30 to 120 nm. CeO_2 NPs stability can also be ascertained using DLS analysis, which helps confirm that the NPs are aggregated in the suspension. The hydrodynamic size, in which the CeO_2 NPs are encircled by water molecules, is responsible for the difference between the larger size seen in DLS analysis (114 nm) and transmission electron microscopy (TEM) (38 nm).

Morphology and Chemical Elemental Analysis

The morphological studies showed that the fabricated CeO_2 NPs were formed by agglomeration with a uniform nanobelt-like structure, as illustrated by the surface morphologies of the CeO_2 NPs made utilizing the *V. trifolia* leaf extract (Figure 3a and 3b). The size of the particles was roughly 35–40 nm, which is nearly the same as the particle size found in Scherer's formula through XRD analysis (Saravanakumar et al., 2019; Tao

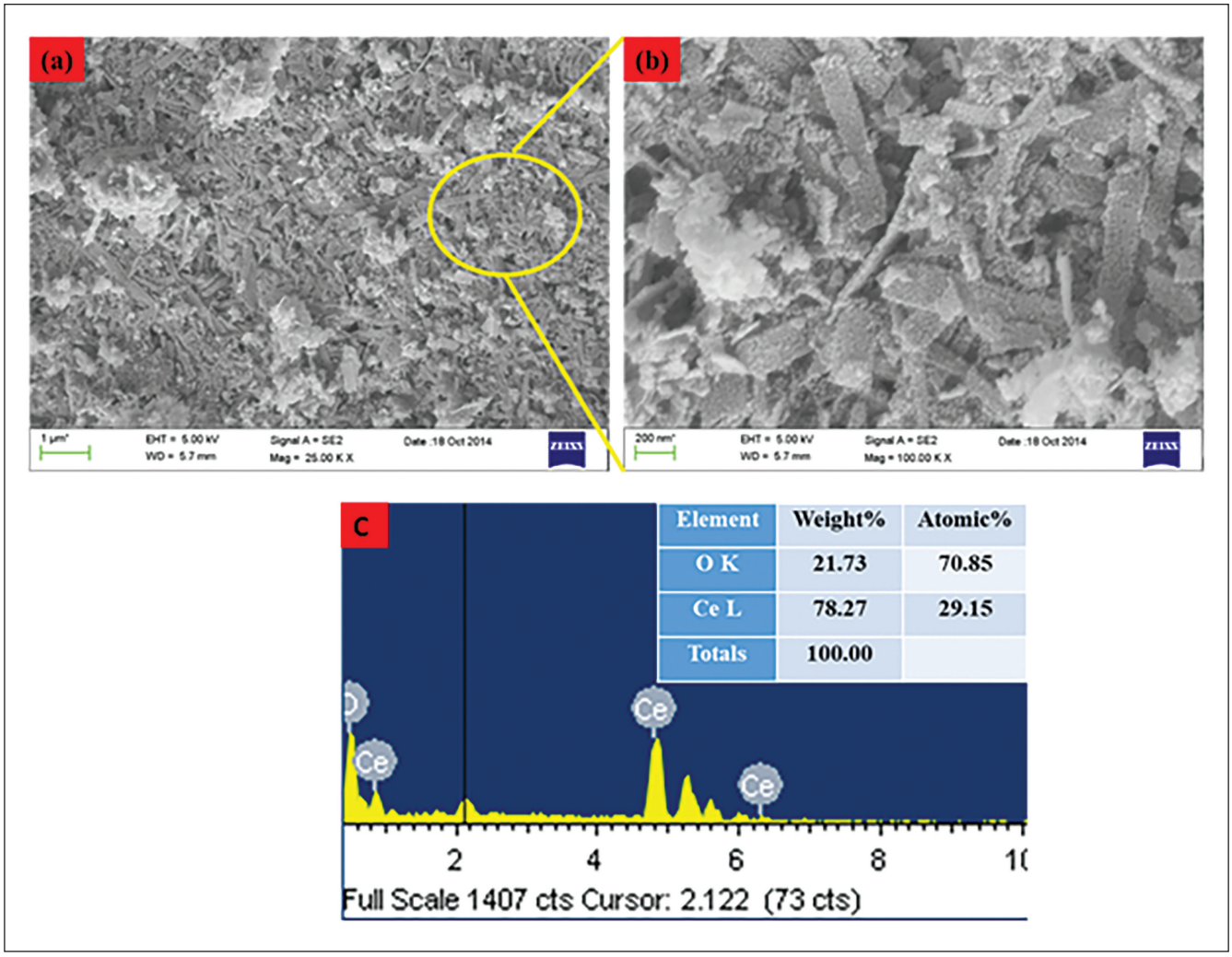


Figure 3. Field Emission Scanning Electron Microscopy (FESEM) Images of Cerium Dioxide Nanoparticles (CeO_2 NPs): Lower (a) and Higher (b) Magnifications, and (c) Energy Dispersive X-ray Analysis (EDAX) Spectrum.

et al., 2008). The size of the particles was found to be 38 nm using ImageJ software. The composition analysis of CeO_2 NPs was carried out using EDAX (Figure 3c). From the EDAX analysis of CeO_2 NPs, the atomic percentages of Ce and O are 29.15% and 78.27%, respectively. There were no other impurities present in the green synthetic CeO_2 NPs.

UV–visible Analysis

The absorption spectra of green-produced CeO_2 NPs, as measured by UV–vis spectroscopy, are shown in Figure 4a. The production of CeO_2 NPs is indicated by the strongest absorption band at 329 nm. The presence of oxidizing polyphenols, which are necessary to prevent CeO_2 NPs from aggregating, is also demonstrated by the expansion band (Saravanakumar et al., 2019). The Plank's formula was used to calculate the bandgap of CeO_2 NPs.

$$Eg = \frac{hc}{\lambda}$$

Where, Eg, bandgap energy (eV), h, Planck's constant (4.1357×10^{-15} eV s), C, velocity of light (2.99×10^{8} m s^{-1}), λ, absorbance peak wavelength (nm). The observed bandgap value was 3.77 eV.

FT-IR Analysis

FT-IR spectroscopy was performed to assess the functional group of the produced CeO_2 NPs. FT-IR spectra (Figure 4b) were detected in the 400–4,000 cm^{-1} wavelength. The bands found were consistent with the earlier studies (Ganesan et al., 2020; Karthik et al., 2022). The hydroxyl and water stretch (O–H stretching) are represented by a prominent absorption band at 3,412 and 1,602 cm^{-1}. The bands noted at 2,913 and 2,819 cm^{-1} arise due to C–H bonding. The bands at 2,354 and 1,361 cm^{-1} may signify the absorption of atmospheric CO_2. The absorption bands at 834, 763, 570, and 436 cm^{-1} signify the Ce–O stretching that confirms the production of CeO_2 NPs.

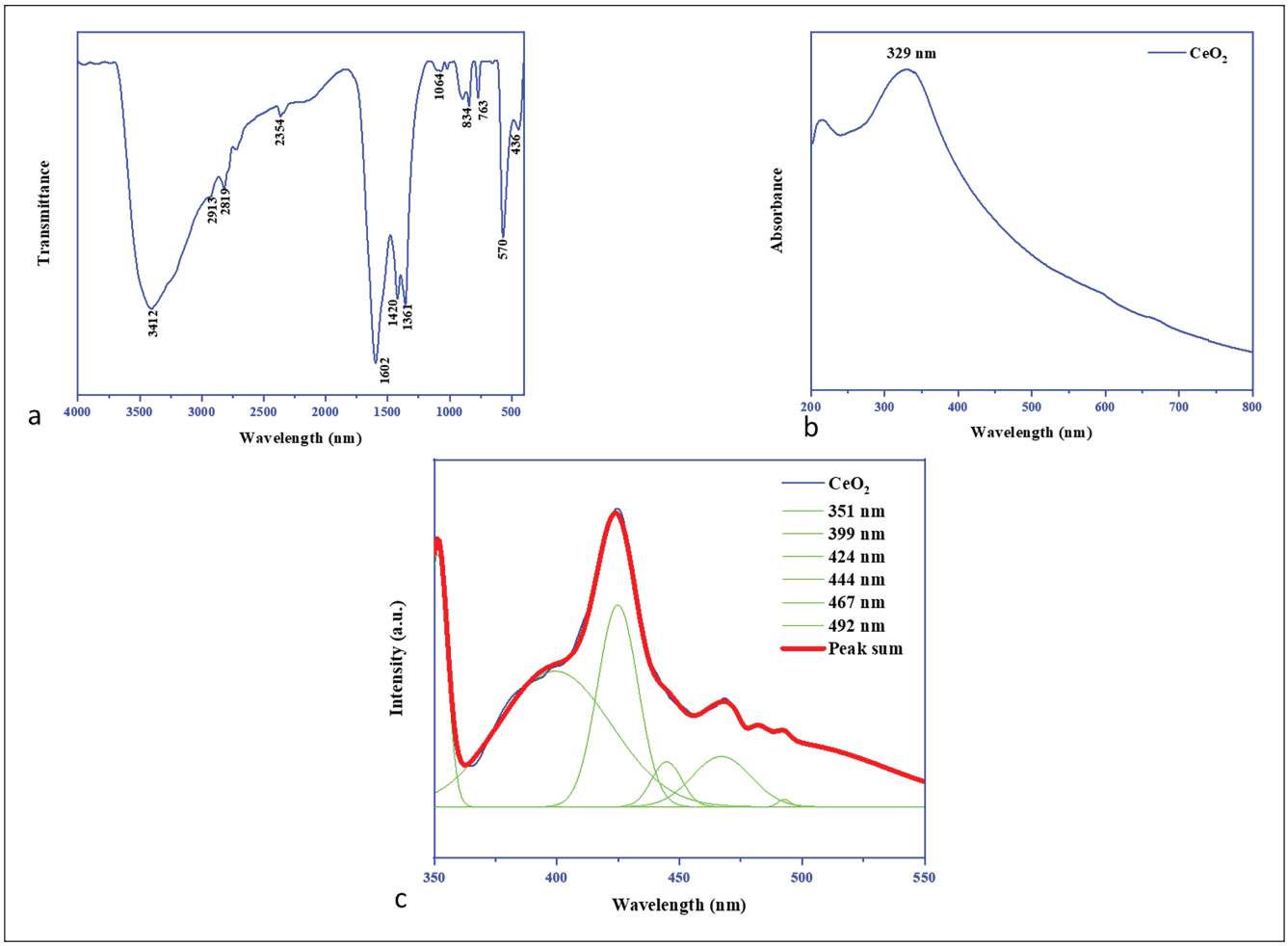


Figure 4. An Analysis of Cerium Dioxide Nanoparticles (CeO_2 NPs) by Ultraviolet (UV) Absorbance (a) Fourier Transform Infrared Spectroscopy (FT-IR) Spectra (b) and (c) Photoluminescence Spectroscopy (PL) Spectra.

PL Studies

The PL spectrum indicates the semiconductor effects of the generated CeO_2 NPs. Consequently, the UV region of the CeO_2 NPs shows weak excitonic emission, while the visible region shows strong emission. Additionally, the excited wavelength at about 325 nm in the PL spectra is related to the emission of CeO_2 NPs. Four peaks (424, 444, 467, and 492 nm) are seen in the blue region of the CeO_2 NPs PL spectrum (Figure 4), which show the emission at 351 nm. In the visible spectrum, a blue emission band was observed at 424, 444, 467, and 492 nm, which could be related to oxygen vacancies. The emission band observed between 350 and 550 nm in wavelength originates from the surface defects (oxygen vacancy) of CeO_2 NPs (Abbas et al., 2020; Mageswari et al., 2016). The transfer of charge carriers from CeO_2 NPs can also shed light on the oxygen vacancies. The PL spectra of CeO_2 NPs made from the leaf extract of *V. trifolia* are shown in Figure 4c.

In Vitro Antioxidant Activity

The *in vitro* antioxidant characteristics of the green-manufactured CeO_2 NPs were examined, and the outcomes are revealed in Figure 5. Here, the *in vitro* antioxidant properties of the CeO_2 NPs rely on the increased doses of the NPs (3.13–200 µg/mL), as mentioned in Figure 5. For CeO_2 NPs, the DPPH scavenging status was found with the increased dosages of the CeO_2 NPs. The study found that the CeO_2 NPs from *V. trifolia* extract showed higher antioxidant effects (IC_{50} 18.06 µg/mL) than the standard vitamin-C (IC_{50} 36.08 µg/mL). This is due to the immense surface-to-volume ratio, which has been shown to function as an antioxidant and free radical scavenger in previous research (Yu et al., 2017). At increasing doses, ZnO NPs have a larger free radical scavenging activity. Nonetheless, our new research suggests that CeO_2 NPs are promising antioxidant options (Lin et al., 2006).

Anti-microbial Activity

The anti-microbial property of green-fabricated CeO_2 NPs treated with different concentrations of (1,000, 1,500, and 2,000 µg/mL) was investigated by the well-diffusion technique against human pathogenic bacteria and fungi such as *S. aureus*, *S. pneumonia*, *B. subtilis*, *K. pneumonia*, *P. aeruginosa*, *V. cholerae*, and *C. albicans* (Figure 6a and 6b). The CeO_2 NPs and the antibiotic amoxicillin exhibited anti-microbial activity. In the case of CeO_2 NPs, increasing the concentration of NPs has also improved their ability to kill microbes.

The anti-microbial mechanism of CeO_2 NPs involves the communication between CeO_2 NPs and microbial cell membranes. The electrostatic attraction of CeO_2 NPs and microbial membranes, adherence to the outer membrane, activation of attacking proteins by the CeO_2 NPs, excessive ROS generation, and the hydrolysis of deoxyribonucleic acid (DNA) oligomers by Ce(IV) ions all contribute to anti-microbial activity (Karakoti et al., 2010; Lin et al., 2006; Pirmohamed et al., 2010; Yu et al., 2017; Zhang et al., 2019). Reactive species such as OH^-, O_2, and H_2O_2 should be synthesized by the reactive agents recombining electron-hole pairs. The electron-donating groups may neutralize the DNA and enzymes by producing cavities (Pirmohamed et al., 2010). CeO_2 NPs have proven to have notable anti-bacterial properties against a variety of bacterial strains. When tested against *E. coli*, CeO_2 NPs showed zones of inhibition ranging from 7 to

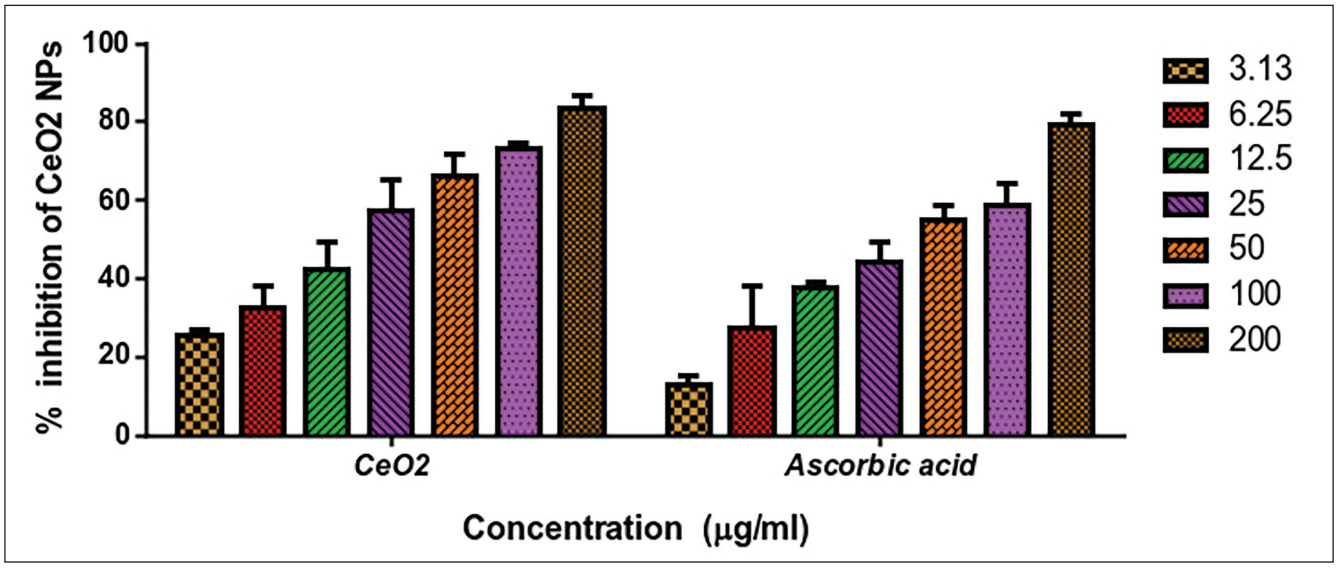


Figure 5. 2,2-Diphenyl-1-picrylhydrazyl (DPPH) Radical Scavenging Action of Cerium Dioxide Nanoparticles (CeO_2 NPs) and Ascorbic Acid. Experiments were Performed in Triplicate to Determine the IC_{50} Value, and Representative Data are Shown Here for the Dose Resulting in 50% Inhibition of Growth.

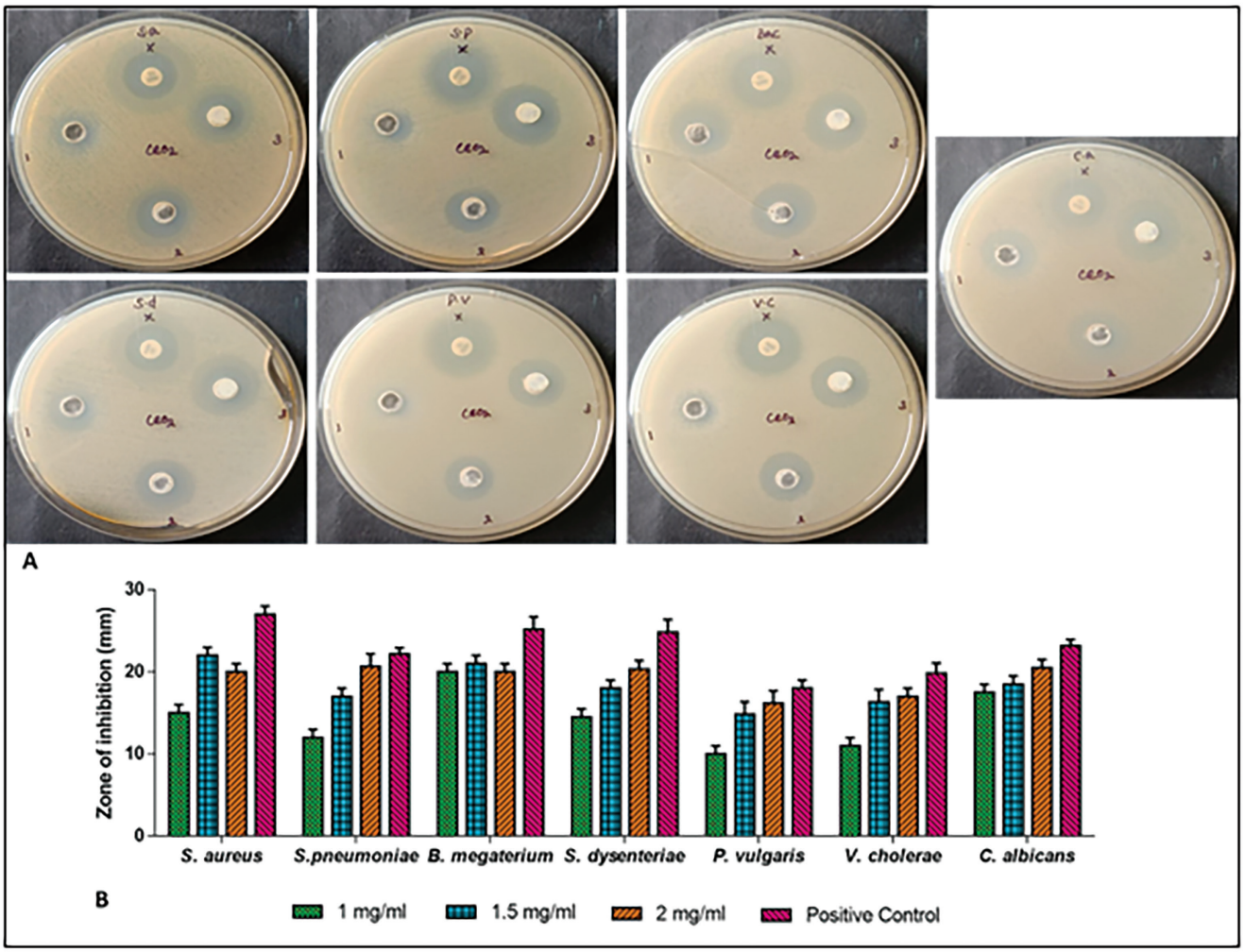


Figure 6. The Results of the Anti-microbial Activity of Cerium Dioxide Nanoparticles (CeO_2 NPs) are Shown. (a) Zones of Inhibition of *Staph aureus*, *Streptococcus pneumonia*, *Bacillus subtilis*, *Klebsiella pneumonia*, *Pseudomonas aeruginosa*, and *Vibrio cholerae* Bacterial Strains were Treated with CeO_2 NPs. (b) A Representative Set of Data from the Triplicate.

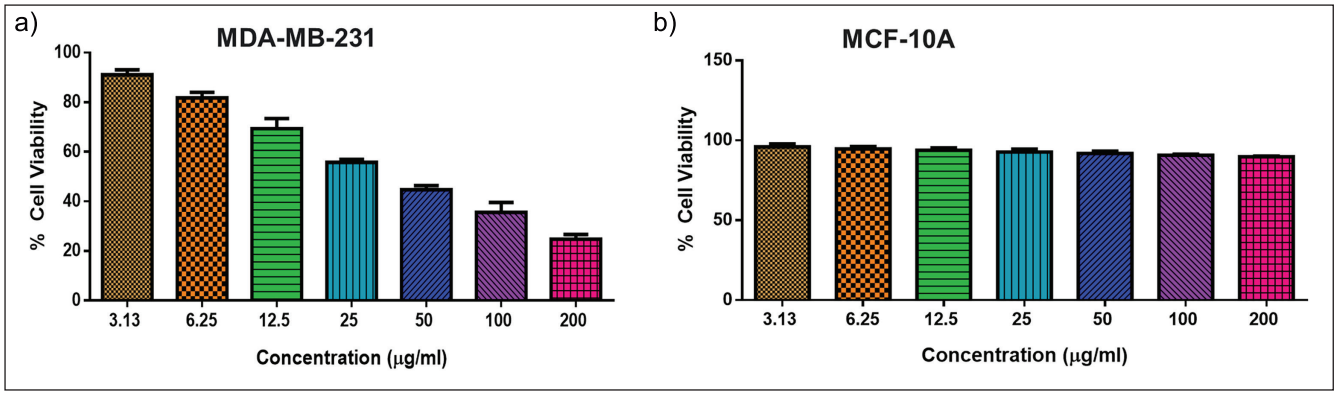


Figure 7. Cytotoxic Assay of Green-synthesized Cerium Dioxide Nanoparticles (CeO_2 NPs) Against MDA-MB-231 (a) and MCF-10A; (b) Cell Lines. The Experiment Shows the Results of a Cell Cytotoxicity Assay Using 3-(4,5-Dimethylthiazol-2-yl)-2,5-Diphenyltetrazolium Bromide (MTT) and CeO_2 NPs at Different Concentrations (200, 100, 50, 25, 12.5, 6.25, and 3.13 µg/mL) in MDA-MB-231 in 96-well Plates. Experiments were Performed in Triplicate to Determine the IC_{50} Value, and Representative Data are Shown Here for the Dose Resulting in 50% Inhibition of Growth.

12 mm. Because of their thicker cell walls, G+ bacterial strains were more resistant to CeO_2 NPs than G− strains (Lord et al., 2012). CeO_2 NPs and chitosan-encapsulated CeO_2 nanocapsules both successfully stopped *E. coli* and *S. aureus* at a 100 µg/mL concentration. When the NPs internalize, oxidative stress is induced, leading to cell death (Das et al., 2013). In similar, CeO_2 NPs showed that they inhibited the growth of *E. coli* and *B. subtilis* at 100 µg/mL, which is caused by the electron-hole pair recombination processes that produce reactive species like hydrogen peroxide, superoxide, and hydroxyl radicals (Niu et al., 2007). Silver coated on the surface of CeO_2 was present in Ag-CeO_2 nanocomposites, which demonstrated anti-bacterial activity against *E. coli*. Both CeO_2 and silver ions contributed to the inhibition of bacterial growth against *E. coli* and *S. aureus* at a concentration of 1,000 µg/mL (Hirst et al., 2009). In addition, TiO_2-CeO_2 nanocomposites demonstrated a significant 19.8 mm inhibition zone against *C. albicans*. The positively charged CeO_2 NPs and the negatively charged cell membranes interact electrostatically in the suggested mechanism, which inhibits cellular transport processes (Colon et al., 2010).

Cell Viability by MTT Assay

The characteristics of CeO_2 NPs were initially evaluated using MTT assays on MDA-MB-231 and MCF-10A cell lines. The results showed that CeO_2 NPs had an IC_{50} of 40.51 µg/mL in MDA-MB-231 cells, while a higher IC_{50} value was observed in MCF-10A cells. Consequently, we treated cells for 24 h at an IC_{50} concentration of 20 and 40 µg/mL in all future tests to evaluate their anti-cancer efficacy before gathering the drug-surviving cells (Figure 7a and 7b). When compared to normal human cells, the outcomes of our MTT analysis revealed that the cell viability was drastically diminished by the green-manufactured CeO_2 NPs treatment, which may be due to the excessive generation of ROS mediated by CeO_2 NPs (Kwon et al., 2016). As a result, it can be stated that green-manufactured CeO_2 NPs have a potential cytotoxic property. It was also discovered that when cancer cells were treated with 40 µg/mL, their viability was reduced by half, and these breast cancer cells were studied further.

Analysis of Apoptosis by AO/EB Staining

CeO_2 NPs were administered to MDA-MB-231 cells at doses of 20 and 40 µg for 24 h, resulting in significantly increased staining with AO/EtBr compared to control cells, which showed basal level staining due to physical stress during cell culture (Figure 8). Increasing apoptosis becomes a crucial target of treatment for various cancers since apoptosis plays an imperative role in the body's homeostasis by eliminating unwanted cells, and so promoting apoptosis becomes an essential feature of cancer therapy (Kuchma et al., 2010). Here, our findings revealed the excellent apoptosis-stimulating property of green-manufactured CeO_2 NPs in both 20 and 40 g/mL dosages. As with some previous research, our study also demonstrated the process of green-synthesized CeO_2 NPs from the *V. trifolia* and their anti-cancerous efficacies against breast cancer by the induction of apoptotic cell death (Kim & Jang, 2019; Wu et al., 2019).

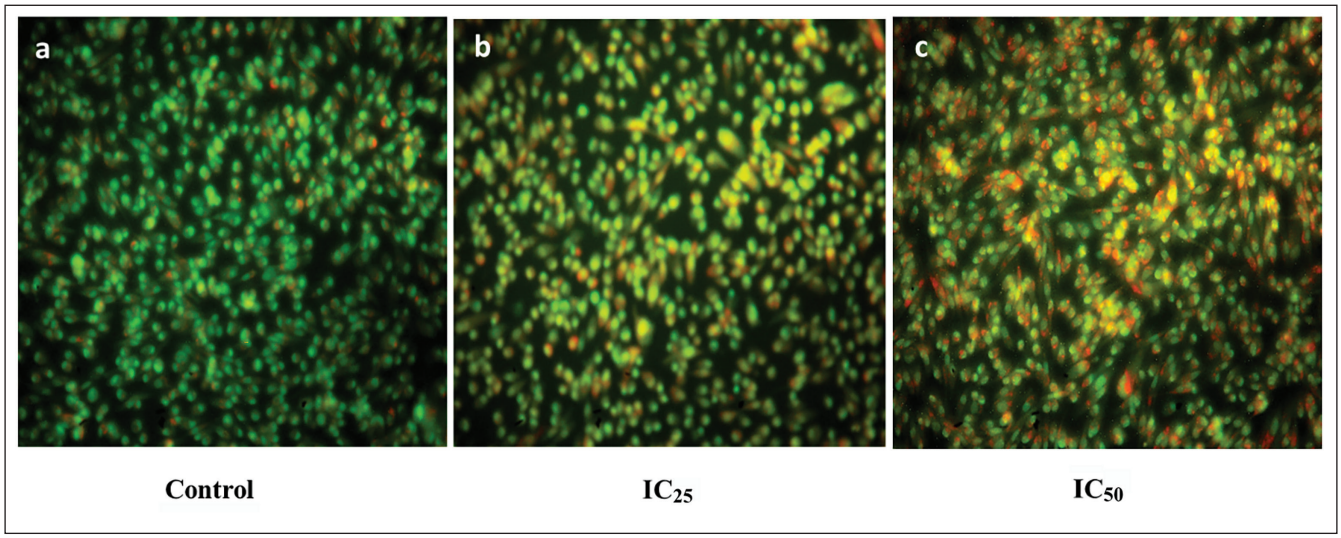


Figure 8. Apoptosis was Determined in MDA-MB-231 Cells by Using Acridine Orange (AO)/Ethidium Bromide (EtBr) Dual Staining with IC_{25} and IC_{50} Doses of Cerium Dioxide Nanoparticles (CeO_2 NPs) After 24 h of Treatment. Cells in Green Color Indicate Live Cells, Yellowish Red Color Cells Indicate Early Apoptotic Cells, and Red Color Cells Indicate Late Apoptotic Cells. Control Cells (a) Cells Treated with 20 µg (IC_{25}) (b) and 40 µg (IC_{50}) (c) of CeO_2 NPs. This is a Representative Image of the Experiment Performed in Triplicate with Magnification at 20×.

Intracellular ROS Generation Analysis

MDA-MB-231 cells were exposed to CeO_2 NPs for 24 h, and the amount of ROS was higher between 12 and 24 h when compared with the control cells. Measurement of ROS was carried out thrice in independent replicates, and mean values are represented in the form of a bar graph as shown in Figure 9. Excessive amounts of ROS are one of the known causes leading to massive DNA damage and cell cycle arrest, and thus to cell apoptosis (Figure 9). Excess ROS is a well-established cause that contributes to serious DNA injury and disruption of the cell cycle, ultimately leading to cell apoptosis (Hussain et al., 2012). We measured the status of ROS control and treated (20 and 40 µg/mL of CeO_2 NPs) MDA-MB-231 cells, and results showed that the CeO_2 NPs treatments drastically increased the ROS production in the MDA-MB-231 cells.

Analysis of MMP Level

MDA-MB-231 cells are grown overnight and treated with CeO_2 NPs for up to 24 h. The cells show a drastic decrease in MMP compared to control cells, with experiments conducted in triplicate and independently each time (Figure 10). MMP is essential for maintaining mitochondrial membrane integrity, and the drop in MMP levels during cell culture apoptosis causes ROS production (Alpaslan et al., 2017). In line with previous research, our findings showed a significant reduction in MMP in malignant cells after supplementation with 20 and 40 µg/mL CeO_2 NPs from *V. trifolia*. In previous studies, similarly, non-small cell lung cancer (NSCLC) is a major cause of cancer-related deaths. Plumbagin, a naturally occurring naphthoquinone, has potential anti-cancer effects. Advancements in sequencing technologies and computational methods have helped predict immunogenic neoantigens, enabling personalized therapies (Sharifi-Rad et al., 2021; Singh et al., 2014).

This study successfully demonstrates the green synthesis of CeO_2 NPs using *V. trifolia* leaf extract, offering an eco-friendly, cost-effective, and biocompatible alternative to conventional synthetic methods. The novelty of this work lies in employing *V. trifolia*, a plant not commonly used in nanoparticle synthesis, to produce CeO_2 NPs with distinct nanobelt-like morphology and well-defined cubic crystalline structures, as confirmed by multiple characterization techniques (XRD, FT-IR, DLS, UV–vis, FESEM, EDAX, and PL). Notably, the synthesized CeO_2 NPs exhibited promising anti-microbial properties, effectively inhibiting the growth of various human pathogens, thereby indicating their potential as green nano-antibiotics. Furthermore, the *in vitro* cytotoxicity assays have revealed selective anti-cancer activity against MDA-MB-231 breast cancer cells, with minimal toxicity observed in non-cancerous cells. The use of AO/EtBr dual staining confirmed that CeO_2 NPs induced apoptotic cell death, highlighting their potential role in targeted cancer therapy. Despite these promising findings, the study has certain limitations. The *in vitro* results need to be validated through *in vivo* models to confirm therapeutic efficacy and biosafety. Additionally, the precise molecular mechanisms underlying the cytotoxic effects and anti-microbial action of the CeO_2 NPs warrant further investigation. Future research should also focus on dose optimization, long-term toxicity, and biodistribution to fully assess the translational potential of these green-synthesized NPs. In summary, this study provides a novel and sustainable approach to synthesizing CeO_2 NPs with demonstrated anti-microbial and anti-cancer potential, paving the way for future biomedical applications with reduced environmental impact.

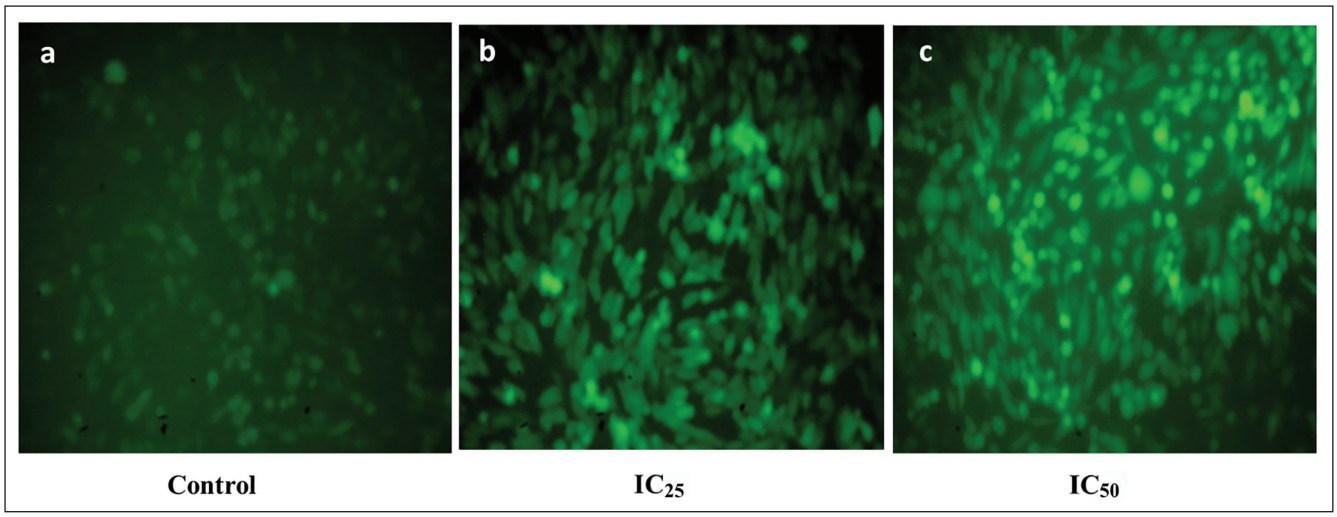


Figure 9. A Fluorescence Microscope Image of Intracellular Reactive Oxygen Species (ROS) Generation Induced by Cerium Dioxide Nanoparticles (CeO_2 NPs) Stained with Dichloro-Dihydro-Fluorescein Diacetate (DCFH-DA). Control Cells (a) Cells Treated with 20 µg (IC_{25}) (b) and 40 µg (IC_{50}) (c) of CeO_2 NPs. This is a Representative Image of the Experiment Performed in Triplicate with Magnification at 20×.

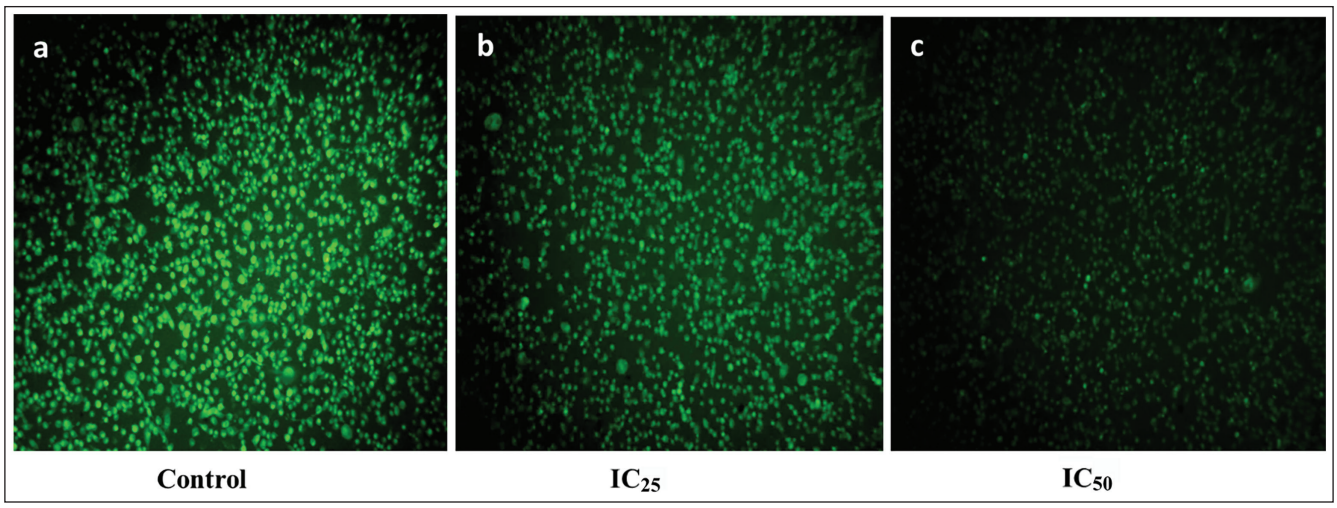


Figure 10. In MDA-MB-231 Cells Treated for 24 h with Cerium Dioxide Nanoparticles (CeO_2 NPs), Mitochondrial Membrane Potential was Determined by Rhodamine 123 Nuclear Staining. Control Cells (a) Cells Treated with 20 µg (IC_{25}) and (b) and 40 µg (IC_{50}) (c) of CeO_2 NPs. This is a Representative Image of the Experiment Performed in Triplicate with Magnification at 20×.

Conclusion

Green-synthesized CeO_2 NPs were successfully produced using *V. trifolia* leaf extract, showcasing a cubic structure with an average size of 34 nm. The NPs formed a nanobelt-like structure with a uniform grain boundary. EDAX analysis confirmed the elemental composition, while FT-IR spectroscopy identified metal-oxygen stretching bands at specific frequencies. UV–visible spectroscopy showed an absorbance band at 329 nm, and the PL spectrum indicated surface defects in the 350–550 nm range. These NPs demonstrated antioxidant and anti-microbial properties, suggesting potential as biocidal agents in biomedical applications. Testing on MDA-MB-231 cells revealed strong cytotoxicity at higher concentrations (3.13–200 µg/mL), with bactericidal activity against various strains.

Authors Contribution

AAA and AHH were involved in the investigation, methodology, and writing—original draft preparation; A.H. reviewed and edited the final version of the manuscript. MAM and SKS were involved in conceptualization, methodology, writing—review & editing, and supervision. The authors read and approved the final manuscript.

Declaration of Conflicting Interests

The authors declared no potential conflicts of interest with respect to the research, authorship, and/or publication of this article.

Ethical Approval

Ethical approval was obtained from the relevant ethics committee or Institutional Review Board (IRB).

Funding

This project was funded by the National Plan for Science, Technology and Innovation (MAARIFAH), King Abdul-Aziz City for Science and Technology, Kingdom of Saudi Arabia (Grant No. 15-BIO4955-02).

ORCID iD

Murugan A. Munusamy https://orcid.org/0000-0001-7792-1797

References

Abbas, M., Samir, H., El-Hamshary, H., El-Newhy, M., & El-Naggar, M. E. (2020). Multifunctional cerium oxide nanoparticles decorated electrospun nanofibers based on chitosan/poly (lactic acid) for wound healing applications. *International Journal of Biological Macromolecules*, *155*, 1558–1570.

Alpaslan, E., Yazici, H., Golshan, N. H., Ziemer, K. S., & Webster, T. J. (2017). PH-controlled cerium oxide nanoparticle inhibition of both gram-positive and gram-negative bacteria growth. *Scientific Reports*, *7*, 45859.

AlSheikh, H. M. A., Sultan, I., Kumar, V., Rather, I. A., Al-Sheikh, H., Tasleem Jan, A., & Haq, Q. M. R. (2020). Plant-based phytochemicals as possible alternative to antibiotics in combating bacterial drug resistance. *Antibiotics*, *9*(8), 480.

Arumugam, A., Karthikeyan, C., Hameed, A. S. H., Gopinath, K., Gowri, S., & Karthika, V. (2015). Synthesis of cerium oxide nanoparticles using *Gloriosa superba* L. leaf extract and their structural, optical and antibacterial properties. *Materials Science and Engineering: C*, *49*, 408–415.

Asati, A., Santra, S., Kaittanis, C., & Perez, J. M. (2010). Surface-charge-dependent cell localization and cytotoxicity of cerium oxide nanoparticles. *ACS Nano*, *4*(9), 5321–5331.

Chan, E. W. C., Wong, S. K., & Chan, H. T. (2018). Casticin from *Vitex* species: A short review on its anticancer and

anti-inflammatory properties. *Journal of Integrative Medicine*, *16*(3), 147–152.

Charbgoo, F., Ahmad, M. B., & Darroudi, M. (2017). Cerium oxide nanoparticles: Green synthesis and biological applications. *International Journal of Nanomedicine*, *12*, 1401–1413.

Chen, F., Zhang, X. H., Hu, X. D., Zhang, W., Lou, Z. C., Xie, L. H., Liu, P. D., & Zhang, H. Q. (2015). Enhancement of radiotherapy by ceria nanoparticles modified with neogambogic acid in breast cancer cells. *International Journal of Nanomedicine*, *10*, 4957–4969.

Chinnasamy, R., Chinnaperumal, K., Arumugam, P., Natarajan, M., Govindasamy, B., Jogikalmat, K., Cherian, T., Kannupaiyan, J., Sigamani, S., & Willie, P. (2024). Phyto-fabrication of AgNPs using leaf extract of *Vitex trifolia*: Potential to antibacterial, antioxidant, dye degradation, and their evaluation of non-toxicity to *Chlorella vulgaris*. *Biomass Conversion and Biorefinery*, *14*, 14903–14920.

Colon, J., Hsieh, N., Ferguson, A., Kupelian, P., Seal, S., Jenkins, D. W., & Baker, C. H. (2010). Cerium oxide nanoparticles protect gastrointestinal epithelium from radiation-induced damage by reduction of reactive oxygen species and upregulation of superoxide dismutase 2. *Nanomedicine*, *6*(5), 698–705.

Das, S., Dowding, J. M., Klump, K. E., McGinnis, J. F., Self, W., & Seal, S. (2013). Cerium oxide nanoparticles: Applications and prospects in nanomedicine. *Nanomedicine*, *8*(9), 1483–1508.

Deshpande, S., Patil, S., Kuchibhatla, S. V. N. T., & Seal, S. (2005). Size dependency variation in lattice parameter and valency states in nanocrystalline cerium oxide. *Applied Physics Letters*, *87*(13), 133113.

Fesenko, T. V., Laguta, I. V., Stavynska, O. M., & Oranska, O. I. (2020). Synthesis of cerium oxide nanoparticles using *Vitex* extract. *Khim Fiz Tekhnol Poverkhni*, *11*, 477–483.

Ganesan, R., Rajeshkumar, S., & Lakshmi, T. (2020). Anticancer and antimicrobial efficacy of cerium oxide nanoparticles synthesized using *Ocimum tenuiflorum* leaf extract. *Journal of Evolution of Medical and Dental Sciences*, *9*(36), 2638–2642.

Hirst, S. M., Karakoti, A. S., Tyler, R. D., Sriranganathan, N., Seal, S., & Reilly, C. M. (2009). Anti-inflammatory properties of cerium oxide nanoparticles. *Small*, *5*(24), 2848–2856.

Hossain, M. M., Paul, N., Sohrab, M. H., Rahman, E., & Rashid, M. A. (2001). Antibacterial activity of *Vitex trifolia*. *Fitoterapia*, *72*(6), 695–697.

Hussain, S., Al-Nsour, F., Rice, A. B., Marshburn, J., Yingling, B., Ji, Z., Zink, J. I., Walker, N. J., & Garantziotis, S. (2012). Cerium dioxide nanoparticles induce apoptosis and autophagy in human peripheral blood monocytes. *ACS Nano*, *6*(7), 5820–5829.

Kamal, N., Mio Asni, N. S., Rozlan, I. N. A., Mohd Azmi, M. A. H., Mazlan, N. W., Mediani, A., Baharum, S. N., Latip, J., Assaw, S., & Edrada-Ebel, R. A. (2022). Traditional medicinal uses, phytochemistry, biological properties, and health applications of *Vitex* sp. *Plants*, *11*(15), 1944.

Kannathasan, K., Senthilkumar, A., Chandrasekaran, M., & Venkatesalu, V. (2007). Differential larvicidal efficacy of four species of *Vitex* against *Culex quinquefasciatus* larvae. *Parasitology Research*, *101*, 1721–1723.

Karakoti, A. S., Singh, S., Dowding, J. M., Seal, S., & Self, W. T. (2010). Redox-active radical scavenging nanomaterials. *Chemical Society Reviews*, *39*(11), 4422–4432.

Karthik, R., Siva, D., Rajeshkumar, S., Venkat Kumar, S., Roy, A., & Lee, J. (2022). Synthesis, characterization, and antibacterial study of cerium oxide nanoparticles synthesized using *Garcinia mangostana* fruit rind extract. *Materials Today Communications*, *31*, 103590.

Karthikeyan, C., Sisubalan, N., Varaprasad, K., Aepuru, R., Yallapu, M. M., Viswanathan, M. R., Umaralikhan, & Sadiku, R. (2022). Hybrid nanoparticles from chitosan and nickel for enhanced biocidal activities. *New Journal of Chemistry*, *46*(27), 13240–13248.

Kim, Y., & Jang, H. H. (2019). Role of cytosolic 2-Cys Prx1 and Prx2 in redox signaling. *Antioxidants*, *8*(6), 169.

Kuchma, M. H., Komanski, C. B., Colon, J., Teblum, A., Masunov, A. E., Alvarado, B., Babu, S., Seal, S., Summy, J., & Baker, C. H. (2010). Phosphate ester hydrolysis of biologically relevant molecules by cerium oxide nanoparticles. *Nanomedicine*, *6*(6), 738–744.

Kwon, H. J., Cha, M. Y., Kim, D., Kim, D. K., Soh, M., Shin, K., Hyeon, T., & Mook-Jung, I. (2016). Mitochondria-targeting ceria nanoparticles as antioxidants for Alzheimer's disease. *ACS Nano*, *10*(2), 2860–2870.

Lan, S., Sheng, X., Lu, Y., Li, C., Zhao, S., & Liu, N. (2018). Modification of antibacterial ZnO nanorods with CeO_2 nanoparticles: Role of CeO_2 in impacting morphology and antibacterial activity. *Colloid and Interface Science Communications*, *26*, 32–38.

Li, W. X., Cui, C. B., Cai, B., Wang, H. Y., & Yao, X. S. (2005). Flavonoids from *Vitex trifolia* L. inhibit cell cycle progression at G2/M phase and induce apoptosis in mammalian cancer cells. *Journal of Asian Natural Products Research*, *7*(4), 615–626.

Li, L., Yang, H. K., Moon, B. K., Fu, Z., Guo, C., Jeong, J. H., Soo, S., Jang, K., & Lee, H. S. (2009). Photoluminescence properties of CeO_2:Eu^{3+} nanoparticles synthesized by a sol-gel method. *Journal of Physical Chemistry C*, *113*(2), 610–617.

Lin, W., Huang, Y. W., Zhou, X. D., & Ma, Y. (2006). Toxicity of cerium oxide nanoparticles in human lung cancer cells. *International Journal of Toxicology*, *25*(6), 451–457.

Lord, M. S., Jung, M., Teoh, W. Y., Gunawan, C., Vassie, J. A., Amal, R., & Whitelock, J. M. (2012). Cellular uptake and reactive oxygen species modulation of cerium oxide nanoparticles in human monocyte cell line U937. *Biomaterials*, *33*(31), 7915–7924.

Mageswari, A., Subramanian, P., Baskar, R., & Natarajan, T. S. (2016). Cerium oxide nanoparticles synthesized by hydrothermal method and their antibacterial activity against pathogenic microorganisms. *Applied Nanoscience*, *6*(5), 651–659.

Majumder, M. A. A., Singh, K., Hilaire, M. G. S., Rahman, S., Sa, B., & Haque, M. (2020). Tackling antimicrobial resistance by promoting antimicrobial stewardship in medical and allied health professional curricula. *Expert Review of Anti-infective Therapy*, *18*(12), 1245–1258.

Munusamy, M. A., Bharathi, M., Alarfaj, A. A., Hussein-Al-Ali, S. H., & Sarathbabu, S. (2024). Pluronic F-127 coated zinc oxide nanoparticles from *Gynura pseudochina*: A comprehensive assessment of antibacterial and anticancer activities. *Journal of Biomaterials Science, Polymer Edition*, *36*(7), 872–891.

Nikolova, M. P., & Chavali, M. S. (2020). Metal oxide nanoparticles as biomedical materials. *Biomimetics*, *5*(2), 27.

Ningaraju, S., Jagadish, K., Srikantaswamy, S., Prakash, A. P. G., & Ravikumar, H. B. (2019). Synthesis of graphite oxide

nanoparticles and conductivity studies of PSF/GO and PSAN/GO polymer nanocomposites. *Materials Science and Engineering: B*, *246*, 62–75.

Niu, J., Azfer, A., Rogers, L. M., Wang, X., & Kolattukudy, P. E. (2007). Cardioprotective effects of cerium oxide nanoparticles in a transgenic murine model of cardiomyopathy. *Cardiovascular Research*, *73*(3), 549–559.

Pirmohamed, T., Dowding, J. M., Singh, S., Wasserman, B., Heckert, E., Karakoti, A. S., King, J. E., Seal, S., & Self, W. T. (2010). Nanoceria exhibit redox state-dependent catalase mimetic activity. *Chemical Communications*, *46*(16), 2736–2738.

Rahdar, A., Aliahmad, M., Samani, M., HeidariMajd, M., & Susan, M. A. B. H. (2019). Synthesis and characterization of highly efficacious Fe-doped ceria nanoparticles for cytotoxic and antifungal activity. *Ceramics International*, *45*(6), 7950–7955.

Ravishankar, T. N., Ramakrishnappa, T., Nagaraju, G., & Rajanaika, H. (2015). Synthesis and characterization of CeO_2 nanoparticles via solution combustion method for photocatalytic and antibacterial activity studies. *Chemistry Open*, *4*(2), 146–154.

Sarathbabu, S., Marimuthu, S. K., Ghatak, S., Vidyalakshmi, S., Gurusubramanian, G., Ghosh, S. K., Subramanian, S., Zhang, W., & Kumar, N. S. (2019). Induction of apoptosis by pierisin-6 in HPV positive HeLa and HepG2 cancer cells is mediated by the caspase-3 dependent mitochondrial pathway. *Anti-Cancer Agents in Medicinal Chemistry*, *19*(3), 337–346.

Saravanakumar, K., Shanmugam, S., Varukattu, N. B., MubarakAli, D., Kathiresan, K., & Wang, M. H. (2019). Biosynthesis and characterization of copper oxide nanoparticles from *Indigofera tinctoria* and its protective effect against H_2O_2-induced oxidative damage in human lung epithelial (A549) cells. *Biotechnology Reports*, *24*, e00368.

Senthilkumar, R. P., Bhuvaneshwari, V., Ranjithkumar, R., Sathiyavimal, S., Malayaman, V., & Chandarshekar, B. (2017). Synthesis, characterization and antibacterial activity of hybrid chitosan-cerium oxide nanoparticles as bionanomaterials. *International Journal of Biological Macromolecules*, *104*, 1746–1752.

Sharifi-Rad, J., Quispe, C., Butnariu, M., Rotariu, L. S., Sytar, O., Sestito, S., Rapposelli, S., Akram, M., Iqbal, M., Krishna, A., Kumar, N. V. A., Braga, S. S., Cardoso, S. M., Jafernik, K., Ekiert, H., Cruz-Martins, N., Szopa, A., Villagran, M., Mardones, L., … Calina, D. (2021). Chitosan nanoparticles as a promising tool in nanomedicine with particular emphasis on oncological treatment. *Cancer Cell International*, *21*(1), 318.

Singh, R., Smitha, M. S., & Singh, S. P. (2014). The role of nanotechnology in combating multi-drug resistant bacteria. *Journal of Nanoscience and Nanotechnology*, *14*(7), 4745–4756.

Soren, S., Jena, S. R., Samanta, L., & Parhi, P. (2015). Antioxidant potential and toxicity study of the cerium oxide nanoparticles synthesized by microwave-mediated synthesis. *Applied Biochemistry and Biotechnology*, *177*, 148–161.

Tao, Y., Gong, F. H., Wang, H., Wu, H. P., & Tao, G. L. (2008). Microwave-assisted preparation of cerium dioxide nanocubes. *Materials Chemistry and Physics*, *112*(3), 973–976.

Ventola, C. L. (2015). The antibiotic resistance crisis: Part 1: Causes and threats. *Pharmacology & Therapeutics*, *40*(4), 277–283.

Wang, L., Hu, C., & Shao, L. (2017). The antimicrobial activity of nanoparticles: Present situation and prospects for the future. *International Journal of Nanomedicine*, *12*, 1227–1249.

Wu, C., Li, H., Wang, T., Gao, Y., Li, J., & Li, S. (2019). Cerium oxide nanoparticles inhibit the migration and invasion of hepatocellular carcinoma cells via suppressing the TGF-β1/Smad2/3 signaling pathway. *International Journal of Nanomedicine*, *14*, 6191–6203.

Yasir, M., Singh, J., Tripathi, M. K., Singh, P., & Shrivastava, R. (2017). Green synthesis of silver nanoparticles using leaf extract of common arrowhead houseplant and its anticandidal activity. *Pharmacognosy Magazine*, *13*(4), S840– S844.

Yu, H., Wu, J., Li, J., Li, X., & Li, Y. (2017). CeO_2 nanoparticles suppress migration and invasion of hepatocellular carcinoma cells through downregulating the expression of matrix metalloproteinases. *Journal of Nanoscience and Nanotechnology*, *17*(3), 1904–1910.

Zhang, M., Zhang, C., Zhai, X., Luo, F., Du, Y., & Yan, C. (2019). Antibacterial mechanism and activity of cerium oxide nanoparticles. *Science China Materials*, *62*(11), 1727–1739.